

1 **Disentangling object category representations driven by dynamic and static**

2 **visual input**

3

4 **Abbreviated Title:** Representation of dynamic and static object information

5

6 Sophia Robert<sup>1,2</sup>, Leslie G. Ungerleider<sup>1</sup>, & Maryam Vaziri-Pashkam<sup>1</sup>

7

<sup>1</sup> Lab of Brain and Cognition, National Institute of Mental Health, Bethesda, MD, USA

8

<sup>2</sup> Department of Psychology and Neuroscience Institute, Carnegie Mellon University, Pittsburgh, PA,

9

USA

10

Corresponding authors: Sophia Robert [srobert@andrew.cmu.edu](mailto:srobert@andrew.cmu.edu) and Maryam Vaziri-Pashkam

11

[maryam.vaziri-pashkam@nih.gov](mailto:maryam.vaziri-pashkam@nih.gov)

12

13 **Number of Pages:** 41

14 **Number of Figures:** 8

15 **Number of Words in Abstract:** 243

16 **Number of Words in Significant Statement:** 120

17 **Number of Words in Introduction:** 635

18 **Number of Words in Discussion:** 1494

19

20 **Conflict of interest statement:** The authors declare no competing financial interests.

21

22 **Acknowledgments:** We thank the late and great Leslie G. Ungerleider for her mentorship and guidance

23 throughout this project, Chris Baker for insightful feedback, and Julian De Freitas for inspiring

24 discussions that helped in forming the initial interest in this research area. This research was supported by

25 the National Institute of Mental Health Intramural Research Program (ZIA-MH-002909).

26

## 27 Abstract

28 Humans can label and categorize objects in a visual scene with high accuracy and speed—a  
29 capacity well-characterized with neuroimaging studies using static images. However, motion is  
30 another cue that could be used by the visual system to classify objects. To determine how  
31 motion-defined object category information is processed in the brain, we created a novel  
32 stimulus set to isolate motion-defined signals from other sources of information. We extracted  
33 movement information from videos of 6 object categories and applied the motion to random dot  
34 patterns. Using these stimuli, we investigated whether fMRI responses elicited by motion cues  
35 could be decoded at the object category level in functionally defined regions of occipitotemporal  
36 and parietal cortex. Participants performed a one-back repetition detection task as they viewed  
37 motion-defined stimuli or static images from the original videos. Linear classifiers could decode  
38 object category for both stimulus formats in all higher order regions of interest. More posterior  
39 occipitotemporal and ventral regions showed higher accuracy in the static condition and more  
40 anterior occipitotemporal and dorsal regions showed higher accuracy in the dynamic condition.  
41 Significantly above chance classification accuracies were also observed in all regions when  
42 training and testing the SVM classifier across stimulus formats. These results demonstrate that  
43 motion-defined cues can elicit widespread robust category responses on par with those elicited  
44 by luminance cues in regions of object-selective visual cortex. The informational content of these  
45 responses overlapped with, but also demonstrated interesting distinctions from, those elicited by  
46 static cues.

## 47 Significance Statement

48 Much research on visual object recognition has focused on recognizing objects in static images.

49 However, motion cues are a rich source of information that humans might also use to categorize

50 objects. Here, we present the first study to compare neural representations of several animate and

51 inanimate objects when category information is presented in two formats: static cues or isolated

52 dynamic cues. Our study shows that while higher order brain regions differentially process object

53 categories depending on format, they also contain robust, abstract category representations that

54 generalize across format. These results expand our previous understanding of motion-derived

55 animate and inanimate object category processing and provide useful tools for future research on

56 object category processing driven by multiple sources of visual information.

## 57 Introduction

58 Humans can categorize objects with striking speed and accuracy. Previous research on  
59 the neural basis of visual object recognition has largely focused on the processing of static  
60 features from images along the ventral visual hierarchy of the primate brain (reviewed in Peissig  
61 & Tarr, 2007). However, real-world scenes are not static. In fact, decades of behavioral research  
62 have shown that motion cues can contain category-relevant information that humans use to make  
63 judgements about objects. Behavioral studies using point-light displays (PLDs, Johansson, 1973;  
64 Johansson, 1976) have established that, even with the impoverished motion information  
65 available in PLDs, humans can quickly perceive a moving person, identify the action being  
66 performed, and even determine the actor's age, gender, and affect (e.g., Barclay et al., 1978;  
67 Bassili, 1978; Cutting and Kozlowski, 1977; Dittrich et al., 1996).

68 The majority of biological motion research has focused on the perception of human  
69 motion due to the significant role that it plays in our social lives. However, our sensitivity to  
70 information in motion cues is not restricted to perceiving humans. Humans can also infer  
71 animacy and complex social relations from the movements of basic geometric shapes (Schultz &  
72 Bühlhoff, 2013; Heider & Simmel, 1944; Scholl & Gao, 2013) and can recognize animal  
73 categories such as chickens, dogs, horses and cats in PLDs (Mitkin & Pavlova, 1990; Mather &  
74 West, 1993; Pinto & Shiffrar, 2009; Pinto, 1994; Pavlova et al., 2001).

75 Investigations of the neural underpinnings of object categorization from motion  
76 information with neuroimaging have identified the superior temporal sulcus (STS) as a key  
77 region involved in processing biological motion. The STS has been shown to track animacy  
78 signals in motion cues from simple shapes and to process dynamic movements of human faces  
79 and bodies (Schultz & Bulthoff, 2013; Hirai & Hiraki, 2006; Pitcher et al. 2011, Pavlova et al.,

80 2004). Neuropsychological studies have also suggested the involvement of parietal regions in the  
81 integration of motion and form information during form-from-motion identification tasks  
82 (Schenk & Zihl, 1997).

83 Despite extensive research into neural substrates of human motion processing (Giese,  
84 2013), there have been comparatively few studies that have investigated how non-human motion  
85 is processed in the brain. Previous studies suggest preferential processing of human motion over  
86 that of one or two other classes, e.g., mammals or tools, in regions in lateral occipito-temporal  
87 cortex (LOTC) including the posterior STS (Papeo et al., 2017), human middle temporal  
88 complex (Kaiser et al., 2012), and fusiform gyrus (Grossman & Blake, 2002), as well as the  
89 inferior parietal lobe, inferior frontal gyrus (Saygin et al., 2004), the posterior and anterior  
90 cingulate cortices and the amygdala (Bonda et al., 1996; Ptito et al., 2003).

91 The limited neuroimaging studies that have directly compared object representations  
92 driven by motion to those driven by static images have focused on human (or monkey) faces and  
93 bodies (Furl et al., 2012; Hafri et al., 2017; Pitcher et al., 2011) or have only compared humans  
94 with tools (Beauchamp et al., 2003). Furthermore, these studies (with the exception of  
95 Beauchamp et al., 2003), have used videos containing both static and dynamic cues as their  
96 dynamic condition and thus have not been able to carefully separate the contributions of motion-  
97 and image-information to the responses. Thus, a systematic comparison of several object  
98 category representations driven by isolated motion and static cues has yet to be undertaken.

99 Here, we devised a novel method to generate stimuli that only contained motion cues. We  
100 extracted motion signals from videos of objects and simulated object movements using flow  
101 fields of moving dots. We first demonstrated that humans can recognize a wide variety of  
102 animate and inanimate objects in our dynamic stimuli. We then used these stimuli, along with

103 static images, in an fMRI study to compare object category representations derived from  
104 dynamic and static cues in occipito-temporal and parietal regions of interest across visual cortex.

## 105 **Materials and Methods**

### 106 **Stimuli**

#### 107 *Stimulus creation pipeline*

108 Eight categories were selected to sample a wide range of animate and inanimate object  
109 categories: human, non-human mammal, bird, reptile, vehicle, tool, pendulum/swing, and ball.  
110 We sought videos of objects performing a wide range of movements. Video clips were  
111 downloaded from various sources on the Internet or shot with in-house equipment in accordance  
112 with the following criteria: 1) contained a single moving object, 2) contained the entire object in  
113 frame without occlusion, 3) shot without camera movement (no zooming, panning, tracking), 4)  
114 contained no movement in the background, and 5) lasted at least 3 seconds.

115 We used in-house Matlab code, the Psychtoolbox extension, and in-house python code to  
116 generate moving dot patterns that followed the movement of the objects in the videos. To do  
117 this, first, all videos were trimmed to 3 seconds, cropped with a 3:2 x/y aspect ratio to center the  
118 object, and resized to 720 x 360 pixel resolution. Videos with 30 frames per second were then  
119 up-sampled so that all videos had a frame rate of 60 fps. The local, frame-by-frame motion of the  
120 objects in each video in x and y directions was then extracted using the Farneback optical flow  
121 algorithm (Farneback, 2003).

122 Next, object movements extracted from the full videos were projected on moving dot  
123 patterns. To create the moving dot stimuli, 2500 white dots (2 pixel diameter) were randomly  
124 initialized on a grey background (360 x 720 pixels). Dots that fell within pixels with nonzero  
125 motion vector values were moved in the direction and magnitude specified by the extracted

126 motion matrix in the next frame. The lifetime (number of contiguous frames of movement) of  
127 any dot was randomly sampled from a uniform distribution between 1 and 17 frames. The  
128 lifetime value decreased on every frame. If the lifetime of a dot reached 0 or they reached the  
129 boundaries of the frame, they were reinitialized with a lifetime of 17 frames.

130 The number of dots for a given frame and their lifetime was set to mitigate the formation  
131 of dot clusters that could induce perception of an edge in individual frames of the video. The  
132 frames were qualitatively examined to see if they induced a perception of any kind of edge or  
133 form. Videos that produced such artifacts were removed from the stimulus set. For the fMRI  
134 experiment, these moving dot videos were rendered live for each trial so that the dot  
135 initializations were always random.

136

### 137 *Stimulus Validation Experiment*

138 To ensure that the stimuli contained clear category information, we conducted an online  
139 experiment. 430 participants (223 women, aged 18-65) were recruited on Amazon Mechanical  
140 Turk to perform an object categorization task on the dynamic stimuli. Participants each  
141 performed between 10-11 trials. For each trial, participants were asked 3 questions about the  
142 object in a looped video: 1) whether the object in the video was of an animal or non-animal, 2)  
143 which of 8 listed categories the object belonged to, and 3) whether they could label the object. If  
144 subjects responded ‘yes’ for the third question, they were required to type the label in a response  
145 text box. Each of the three questions contained an “I don’t know” option. Subjects had to answer  
146 all three questions to complete each trial.

147 Overall, subjects categorized objects based on their motion in the moving dot stimuli with  
148 an average accuracy of 76% (202 total videos). The three animate (human, mammal, reptile) and

149 three inanimate (tool, ball, pendulum/swing) categories with the highest accuracy were used for  
150 the fMRI experiment. For each category, the 6 videos with the highest accuracy were selected  
151 (mean accuracy = 96%).

152 The overall ‘motion energy’ of each video was calculated by averaging the motion  
153 vectors across all pixels in all frames. Non-zero motion vectors were also used to calculate the  
154 average non-zero ‘motion energy’. The average overall and non-zero motion energy for the 6  
155 videos in each category were entered into pairwise two-sample heteroscedastic t-test  
156 comparisons to ensure that there were no significant differences between categories for either  
157 metric. Neither the overall nor the non-zero motion energies were significantly different across  
158 categories (all  $ps > 0.05$ , even without correction for multiple comparisons).

159 After the dynamic video stimulus set was finalized, the static image stimulus set was  
160 generated by randomly selecting three frames of the full form video from which the moving dot  
161 stimulus was created. The frame with the object in clearest view was selected and further  
162 processed to extract the object from the frame. For the fMRI experiment, the isolated object was  
163 pasted onto a background of 2500 randomly initialized white dots on a grey background, to  
164 mimic a frame of the dynamic moving dot stimuli.

165

## 166 **Functional MRI experiment**

### 167 Participants

168 Fifteen healthy human subjects (six women, age range 19-42) with normal or corrected to  
169 normal vision were recruited for the fMRI experiment. Participants were brought in for a 2 h  
170 fMRI session that included the main experiment and three localizer tasks. Prior to entering the  
171 scanner, all participants practiced the tasks for the main experiment and localizer runs and



172 underwent a short behavioral task to familiarize themselves with the stimuli. All subjects  
173 provided informed consent and received compensation for their participation. The experiments  
174 were approved by the NIH ethics committee.

### 175 Training Session

176 The independent norming study performed with mTurk demonstrated that people can  
177 recognize the objects in these stimuli with high accuracy after minimal instruction. However, to  
178 avoid introducing any random factors across subjects and differential processing during the first  
179 run of the session relative to the rest, participants participated in a training session prior to  
180 entering the scanner. During the training session, they familiarized themselves with the 36  
181 dynamic stimuli and were subsequently tested to ensure accurate recognition. Each video was  
182 shown on loop until subjects could verbally report which of the 6 categories the object belonged  
183 to. If the subject categorized the object correctly, the experimenter advanced to the next stimulus;  
184 incorrect categorizations were verbally corrected by the experimenter. After all stimuli had been  
185 verbally categorized, subjects underwent a testing session. In each trial, a random video was  
186 shown once without looping, followed by a grey screen with 6 category labels placed in a circle  
187 around the center of the screen. Subjects were instructed to categorize the object in the video by  
188 clicking on the corresponding category label. No feedback was provided during the testing  
189 session. If a subject performed above 90% accuracy, they continued on to the fMRI experiment.  
190 The training and testing session took no longer than 15 minutes. Subjects required little to no  
191 correction during the training session and performed with an average of 99% accuracy in the test  
192 session on the first iteration (n = 13, data for two subjects were lost due to technical problems).

193

194

195 *MRI Methods*

196 MRI data were collected from a Siemens MAGNETOM Prisma scanner at 3 Tesla  
197 equipped with a 32-channel head coil. Subjects viewed the display on a BOLDscreen 32 LCD  
198 (Cambridge Research Systems, 60 Hz refresh rate, 1600 x 900 resolution, at an estimated  
199 distance of 187 cm) through a mirror mounted on the head coil. The stimuli were presented using  
200 a Dell laptop with MATLAB and Psychtoolbox extensions (Brainard, 1997; Kleiner, Brainard, &  
201 Pelli, 2007).

202 For each participant, a high resolution (1.0 x 1.0 x 1.0 mm) T1-weighted anatomical scan  
203 was obtained for surface reconstruction. All functional scans were collected with a T2\*-weighted  
204 single-shot, multiple gradient-echo EPI sequence (Kundu et al., 2012) with a multiband  
205 acceleration factor of 2 slices/pulse. 50 slices (3 mm thick, 3 x 3 mm<sup>2</sup> in-plane resolution) were  
206 collected to cover the whole brain (TR 2 s, TE = 12 ms, 28.28 ms, 44.56 ms, flip angle = 70°,  
207 FoV = 216 mm).

208 *Experimental Design*

209 **Main Experiment:** The main task of the experiment included 6 categories: human,  
210 mammal, reptile, tool, pendulum/swing, and ball and 2 stimulus conditions: dynamic (moving  
211 dot videos) and static (object images pasted on dot background). Both dynamic and static stimuli  
212 were presented at the same size and location (subtending 9.6° x 4.8° visual angle). We used a  
213 block design to present alternating blocks of dynamic and static stimuli while also alternating  
214 between animate and inanimate blocks. The order of the six categories and the two formats were  
215 counterbalanced within and across runs. Four different counterbalancing designs were created  
216 and each subject was randomly assigned one of the designs.

217 Each run contained 12 condition blocks, one for each condition (2 formats x 6  
218 categories), began with an initial fixation block of 8 s, and ended with a final fixation of 12 s.  
219 Each condition block began with an 8 s fixation period in which a red fixation dot (5 pixels in  
220 radius) was shown on a grey background. The fixation period was then followed by the stimulus  
221 presentation period in which 4 stimuli were presented from the same condition, each for 2.8 s  
222 followed by a 200 ms inter-stimulus interval, resulting in 12 s of stimulus presentation. The  
223 duration of each condition block was 20 s (8 s fixation and 12 s stimulus presentation). For each  
224 run, the 12 condition blocks and the initial and final fixation blocks lasted 252 s (4 min 12 s).  
225 Each participant completed 12 runs.

226 To maintain their attention, subjects were given a one-back repetition detection task in  
227 which they were instructed to press a button on an MRI-compatible button box (fORP,  
228 Cambridge Research Systems) to indicate detection of a repeated stimulus within each block.  
229 There was one stimulus repetition per block and the repeated stimulus of each block type was  
230 changed across runs. Because there were only 3 unique trials per block but each condition had 6  
231 unique stimuli, half of the stimuli of each category were shown on odd runs and the other half  
232 were shown on the even runs. These blocks were later combined during analysis. Average  
233 performance on this task was 94%. To ensure proper fixation, eye movements were monitored  
234 using an ASL eye-tracker.

235 **Object Localizer task:** To localize functional ROIs in ventral and lateral occipito-  
236 temporal cortex, we presented images of objects in 6 conditions: faces, scenes, head-cropped  
237 bodies, central objects, peripheral objects (4 objects per image), and phase-scrambled objects in a  
238 block design paradigm. Subjects were instructed to fixate while 20 images were presented in  
239 each block for 750ms with a 50ms fixation screen in between. Each block lasted 16 s and was

240 repeated 4 times per condition. Each run started with a 12s fixation period. Additional 8 s  
241 fixation periods were presented after every 5 blocks. Total run duration was 436 s (7 min 16 s).  
242 Subjects performed a motion detection task. During each block, a random image would jitter by  
243 rapidly shifting 4 pixels back and forth horizontally from the center of the screen. Subjects  
244 indicated detection of motion with a button press. Each participant completed 1-2 runs of this  
245 task.

246 **Motion localizer task:** To localize functional ROIs related to the perception of biological  
247 and non-biological motion, we presented blocks of point light display (PLD) videos of humans  
248 performing various actions in four conditions: 1) biological motion: normal PLD video (e.g.  
249 walking, riding a bicycle), 2) random motion: the points in the PLD were spatially scrambled in  
250 each frame, 3) translation: randomly positioned dots translated across the screen in a random  
251 direction with the speed set to the average speed of the movement from the PLD videos, and 4)  
252 static: a random frozen frame of the PLD was shown as an image. There were 8 exemplars per  
253 condition, each presented for 1.5 s followed by a 500 ms interstimulus fixation period. Each  
254 block lasted 16 s and was presented 4 times per condition. Each run began with a 6s fixation  
255 period and 8 s fixation periods were interspersed between each block making the total run  
256 duration 422.7 s (7 min 3 s). Subjects performed a one-back repetition detection task, in which  
257 they indicated detection of a repeated stimulus during each block by pressing a button. Each  
258 subject completed 1-2 runs of this task.

259 **Topographic mapping:** Topographic visual region V1 was mapped using 16 s blocks of  
260 a vertical or horizontal polar angle wedge with an arc of 60° flashing black and white  
261 checkerboards at 6 Hz. During the stimulus blocks, subjects fixated on a red fixation dot (5 pixel  
262 radius) and detected a dimming on the wedge, that occurred randomly either at the inner, middle,

263 or outer ring of the wedge at 4 random times within the 16 s block. There was a 16 s fixation  
264 period after each block and each run began with a 16 s period of fixation. Each run lasted 272 s  
265 (4 min and 40 s), and subjects completed 1-2 runs of this task.

#### 266 Data Analysis

267 fMRI data were analyzed using AFNI (Cox, 1996) and in-house MATLAB codes. The  
268 data were pre-processed by removing the first 2 TRs of each run, motion correction, slice timing  
269 correction, smoothing with 5mm FWHM, and intensity normalization. The EPI scans were  
270 registered to the anatomical volume. The three echoes were combined using a weighted average  
271 (Posse et al., 1999; Kundu et al., 2012). TRs with motion exceeding 0.3 mm as well as outliers  
272 were excluded from further analysis. A general linear model analysis with 12 factors (2 stimulus  
273 conditions x 6 categories) was used to extract t-values for each condition in each voxel. The 6  
274 degrees of freedom movement parameters was used as an external regressor. To account for the  
275 effect of residual autocorrelation on statistical estimates, we applied a generalized least squares  
276 time series fit with restricted maximum likelihood (REML) estimation of the temporal auto-  
277 correlation structure in each voxel. The t-values were calculated across all runs for the univariate  
278 analysis and per-run for the multivariate analysis.

#### 279 ROI Definition: Group-constrained subject specific method

280 We used a systematic, unbiased method for creating individualized regions of interest  
281 constrained by group responses to our localizer experiments, basing our approach on a method of  
282 region of interest definition developed by Kanwisher and Fedorenko (described in Kanwisher et  
283 al., 2011).

284 First, t-values were extracted from generalized linear models (GLMs) of individual  
285 activation maps from the localizer experiments. All subjects' statistical activation maps (N = 15)

286 were converted to Talairach space. For each subject, the individual localizer contrast maps were  
287 thresholded at  $p < 0.0001$ . Group overlap proportion maps were then created for each contrast.

288         Second, we thresholded the group proportion maps for each contrast separately to  
289 counteract contrast- or localizer-specific differences in spatial variability or overall activation.  
290 The thresholds for specific contrast maps were as follows: For the object localizer experiment,  
291 the thresholds were  $N \geq 0.7$  for objects vs scrambled (lateral occipital, LO; posterior fusiform  
292 sulcus, pFS),  $N \geq 0.5$  for bodies vs objects (extrastriate body area, EBA), and  $N \geq 0.25$  for  
293 peripheral objects vs scrambled (inferior intraparietal sulcus, infIPS). For the biological motion  
294 experiment, the threshold for biological motion vs translation was  $N \geq 0.5$  (lateral occipito-  
295 temporal biomotion region, LOT-biomotion). For the retinotopy experiment, positive and  
296 negative maps were created separately and thresholded at  $N \geq 0.5$ .

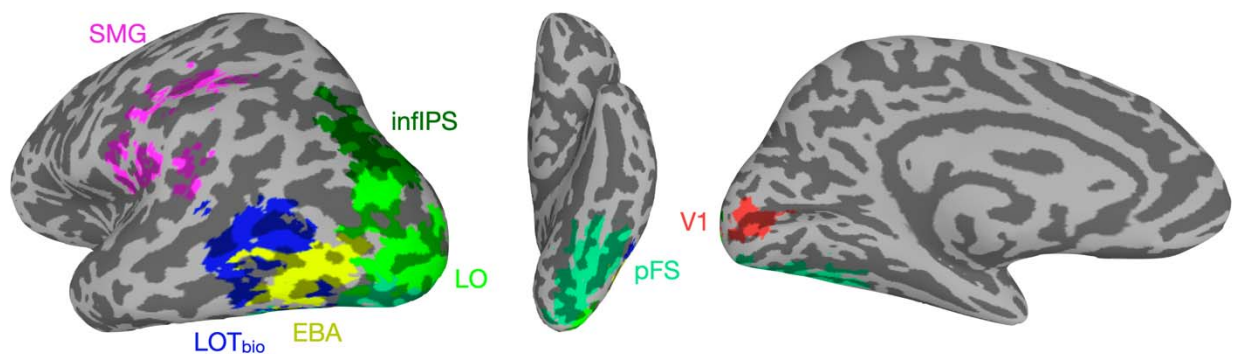
297         Third, we used a Gaussian blur of 1mm FWHM. The blurred maps were then clustered  
298 using the nearest neighbors method and a minimum cluster size of 20 voxels. For V1, positive  
299 and negative maps were clustered separately and then combined with a step function. Two steps  
300 were required to finalize the group-constrained ROIs. Anatomical landmarks were used to  
301 separate pFS from LO, and LO from infIPS. V1 was separated from V2 using a hand-drawn  
302 region based on the group map. All ROIs were then selected to have no overlapping voxels.

303         The final nonoverlapping group-constrained ROIs were made subject specific by creating  
304 masks based on the individual subject's activity during the localizer experiments (localizer  
305 contrast threshold:  $p < 0.05$ ). For example, for each subject's EBA, the group-constrained EBA  
306 was masked by the subject's response to bodies > objects with a threshold of  $p < 0.05$ . If this  
307 process did not yield an ROI with at least 100 voxels across the two hemispheres, the ROI was

308 instead created with a mask made from the mean response during the main experiment (task vs  
309 fix,  $p < 0.0001$  uncorrected).

310 The supramarginal (SMG) region of interest was anatomically defined using a Freesurfer  
311 parcellation (Desikan et al, 2006). To make the subject specific supramarginal ROIs, individual  
312 masks were made from the mean response during the main experiment (task vs fixation,  $p <$   
313  $0.0001$  uncorrected) and intersected with the template SMG region.

314



315 **Figure 1.** Regions of interest of a single example subject generated by the group-constrained single-  
316 subject method. The supramarginal area (SMG) is colored in pink, the inferior intraparietal sulcus  
317 (infIPs) is colored in dark green, the lateral occipital complex (LO) is colored in light green, the  
318 extrastriate body area (EBA) is colored in yellow, the biological motion related lateral occipito-temporal  
319 area (LOT-bio) is colored in dark blue, the posterior fusiform sulcus (pFS) is colored in teal, and primary  
320 visual cortex (V1) is colored in red.

321

### 322 Univariate analysis

323 To calculate the average fMRI response per condition for each ROI, using a general  
324 linear model analysis, whole brain t-value maps were extracted for each of the 12 conditions and  
325 masked with a task > fixation threshold of  $p < 0.0001$  for each subject. The group-constrained  
326 subject-specific ROIs were intersected with these maps, resulting in a t-value response per voxel  
327 in each ROI for all 12 conditions in each subject. The average responses for four conditions were  
328 then calculated from these ROI responses: dynamic animate, dynamic inanimate, static animate,  
329 and static inanimate. The animacy preference in each ROI was calculated as the difference  
330 between the animate and inanimate conditions, separately for the static and dynamic stimulus

331 formats. One-sample and paired t-tests were conducted to determine respectively: 1) if the  
332 animacy preference in each ROI and each format was significantly different from 0, and 2) if the  
333 animacy preference was significantly different across stimulus formats within each ROI. All t-  
334 tests were corrected for multiple comparisons with False Discovery Rate correction (Benjamini  
335 and Hochberg, 1995) across ROIs.

### 336 Multivariate pattern analysis (MVPA)

337 We performed multivariate pattern analyses to investigate whether object category  
338 information was present in the fMRI responses to the dynamic and static stimuli. We extracted t-  
339 values in each voxel for every condition in each run using a GLM analysis. To perform pairwise  
340 object category decoding, we used a linear support vector machine classifier (SVM; Chang and  
341 Lin, 2011) with feature selection. The SVM was trained using leave-one-out cross validation on  
342 data that was normalized with z-scoring to avoid magnitude differences between conditions.  
343 Using t-tests, we calculated the top 100 most informative voxels per ROI (Mitchell et al., 2004)  
344 to equate the number of voxels analyzed per ROI and facilitate comparisons between them. This  
345 feature selection was performed separately for each iteration of training. Results did not  
346 qualitatively change when the analysis was performed without feature selection.

347 We trained and tested the linear SVM in two conditions: 1) within-classification, in  
348 which the SVM was trained and tested on the same stimulus format, and 2) cross-classification,  
349 in which SVM was trained in one stimulus format and tested on the other format. The  
350 classification was performed on all unique pairs of object categories to obtain classification  
351 accuracy matrices. The off-diagonal values of the matrices were averaged to produce two within-  
352 format and two cross-format average object category decoding accuracies per subject. The two  
353 cross-format values were then averaged to obtain one cross-classification accuracy. One-sample



354 and paired t-tests were conducted to determine respectively: 1) if the decoding accuracy in each  
355 ROI and each format was significantly different from chance (0.5), and 2) if the decoding  
356 accuracy was significantly different across stimulus formats within each ROI. All p-values listed  
357 from t-tests and ANOVAs were corrected for multiple comparisons with False Discovery Rate  
358 correction across ROIs (Benjamini and Hochberg, 1995). For ANOVAs, effect sizes were  
359 calculated with generalized eta squared ( $\eta_g^2$ ), for the one sample and paired t-tests, Cohen's  $d$   
360 was used.

### 361 Multidimensional scaling of fMRI responses

362 To visualize how stimulus format and object category impact the responses in our regions  
363 of interest, we quantified the similarities between the patterns of fMRI responses to the 12  
364 conditions in each ROI by calculating all pairwise Euclidean distances. The individual subject  
365 Euclidean distances per ROI were averaged across subjects to create group Euclidean distances,  
366 which will be referred to as the fMRI-Euclidean matrix. We then visualized these similarities by  
367 applying classical multidimensional scaling (Shepard, 1980) on the fMRI-Euclidean matrix and  
368 plotting the first two dimensions for each ROI.

369 We measured the reliability of the fMRI-Euclidean matrix by performing a permutation  
370 analysis wherein the individual subject matrices were split into two groups, averaged to create  
371 two group matrices, and then correlated to get a measure of the split-half reliability. Correlations  
372 for every possible combination of subjects in the two groups were measured and averaged to  
373 produce a final reliability score. The reliabilities of the dynamic and static fMRI-Euclidean  
374 matrices were evaluated separately.

375

376

377

## 378 **Object similarity behavioral experiment**

379 353 participants (32% female among the 85% who responded to the demographic survey)  
380 were recruited on Amazon Mechanical Turk to perform an object similarity task on the dynamic  
381 or static stimuli. All participants were located in the United States.

382 For each trial, participants were presented with three stimuli on a grey screen and were  
383 instructed to select the ‘odd-one-out’ stimulus (the stimulus that was most distinct among the  
384 three) by clicking on it. Dynamic and static stimuli were tested separately. Participants  
385 performed blocks of 15 trials to complete the task and were permitted to perform more than one  
386 block. To ensure data quality, trials with RTs smaller than 0.6 s and 1.2 s and larger than 10 s or  
387 20 s were removed for the image and video tasks, respectively. These cutoffs were decided based  
388 on the distributions of RTs. If 5 or more trials in a block were eliminated, the entire block (or  
389 HIT in mTurk terminology) was removed. The eliminated blocks were resubmitted to mTurk to  
390 ensure that we had at least 2 repetitions for each unique triplet allowing for 68 trials for each pair  
391 of stimuli.

392 To build a dissimilarity matrix based on the odd-one-out image and video tasks, a  
393 response matrix of the pairwise dissimilarity judgments was constructed for each task by treating  
394 each triplet as three object pairs and assigning 1’s to dissimilar pairs (i.e. the two pairs that  
395 included the selected odd object) and a 0 to the similar pair (i.e. the pair that did not include the  
396 selected odd object). We also constructed a count matrix to determine how many times each pair  
397 was shown together in a triplet. By dividing the response matrix by the count matrix, we  
398 obtained a dissimilarity matrix with values ranging from 0-1 with higher values denoting higher  
399 dissimilarity. To produce a category level behavioral dissimilarity matrix, we took the off-

400 diagonal upper triangle of the 36 x 36 matrix and averaged the item distances that belonged to  
401 the same category, resulting in a 6 x 6 matrix, which will be referred to as the behavioral-  
402 dissimilarity matrix. The diagonal was nonzero due to nonzero distances between exemplars  
403 within each category. Only the off-diagonal of this matrix was used in further analyses.

404 To gauge the stability of the behavioral-dissimilarity matrix, we performed a split-half  
405 reliability analysis. Because each subject only saw a small set of all possible triplets, instead of  
406 splitting the data by subject, we split based on repeats of stimulus pairs (3 pairs per triplet) into  
407 two groups. The binary similarity values for all pairs were correlated across the two groups to  
408 produce a measure of reliability of the similarity judgments.

409

#### 410 *Multi-dimensional scaling and hierarchical clustering of object similarity responses*

411 We visualized the structure of the object similarity judgments from the odd-one-out tasks  
412 at the category level using classical multidimensional scaling on the behavioral-dissimilarity  
413 matrices of the dynamic and static stimuli separately (Shepard, 1980). The two behavioral-  
414 dissimilarity matrices were also correlated to quantify their degree of similarity. To investigate  
415 the structure of the object similarity judgments at the exemplar level, we used a hierarchical or  
416 agglomerative clustering algorithm available in the Python package *scipy* (Virtanen et al., 2020)  
417 on the dynamic and static behavioral-dissimilarity matrices separately. For visualization  
418 purposes, images of the individual exemplars, which were adapted from the static stimuli used in  
419 the experiment, were included under the resultant dendrograms for both static and dynamic  
420 conditions (note that dynamic stimuli are not recognizable in static frames).

421

#### 422 *Brain-behavior correlation*

423 To determine the relationship between the multivariate information for the six categories  
424 in each region of interest (fMRI-Euclidean matrix) with behavioral assessments of the category  
425 similarity (behavioral-dissimilarity matrix), we correlated the two measures. For each subject,  
426 the off-diagonal of the fMRI-Euclidean matrix was correlated with the off-diagonal behavioral-  
427 dissimilarity matrix using Pearson's linear correlation coefficient, separately for the dynamic and  
428 static experiments. The correlations were then averaged across subjects. The noise ceiling of  
429 these correlations was then calculated for each ROI as the square root of the product of the  
430 reliabilities of the fMRI-Euclidean matrix and the behavioral-dissimilarity matrix. As the  
431 reliability of the behavioral-dissimilarity matrix was calculated with only one split, the standard  
432 error of the noise ceiling was calculated based on the mean and standard deviation of the  
433 reliability scores generated on each permutation of the fMRI-Euclidean reliability analysis.

434

#### 435 Brain-optic flow correlation

436 To ensure that optic flow information from the six object categories was not predictive of  
437 the multivariate fMRI responses in any of the regions of interest, we performed a control  
438 analysis. We first calculated the Euclidean distances between the dynamic stimulus information  
439 of each category by vectorizing the 4-dimensional stimuli (x-coordinates, y-coordinates, x- and  
440 y-magnitudes of optic flow, and time) and averaging the distances between stimuli of the same  
441 category, creating the optic flow-Euclidean matrix. We then correlated the optic flow-Euclidean  
442 matrix with the dynamic fMRI-Euclidean matrix of each ROI for each subject. The correlations  
443 were averaged across subjects to generate group mean correlations and one-sampled t-tests were  
444 used to determine whether any positive correlations were significantly above zero.

445

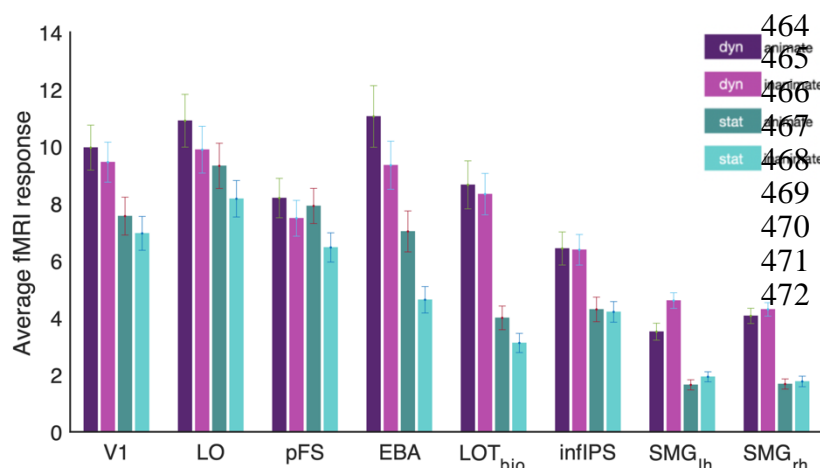
446

447

## 448 Results

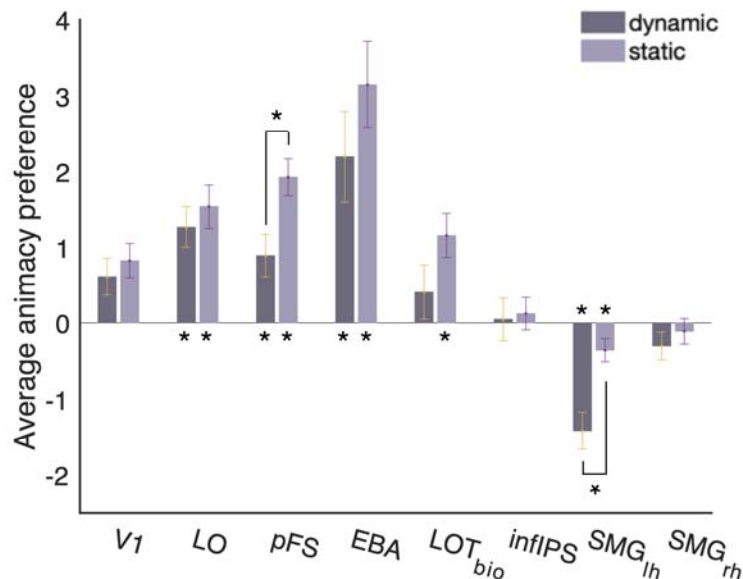
### 449 Effect of stimulus format on univariate animacy preference

450 We first looked at the mean amplitude of responses to the two superordinate object  
451 categories (animate/inanimate) in the two stimulus formats (static/dynamic). We extracted  
452 individual subjects' t-values from the GLM analysis and averaged the response for the three  
453 animate and the three inanimate categories within each image format to get 4 values per subject.  
454 Figure 2 shows the pooled results of this analysis across subjects. A two-way ANOVA with  
455 stimulus format and animacy as factors showed a significant main effect of stimulus format in all  
456 ROIs ( $f_s > 7.26$ ,  $p_s \leq 0.02$ ,  $\eta^2_s > 0.02$ ) with higher response amplitude in the dynamic compared  
457 to the static condition. A main effect of animacy was also found in LO, pFS, EBA, LOT-  
458 biomotion, and left SMG ( $f_s > 7.68$ ,  $p_s < 0.03$ ,  $\eta^2_s > 0.02$ ), but not in V1, infIPS, or right SMG  
459 ( $f_s < 3.38$ ,  $p_s > 0.12$ ,  $\eta^2_s < 0.009$ ). For the four ventrottemporal cortical areas, average responses  
460 were significantly higher for the animate object categories, while in left SMG the average  
461 response was higher for the inanimate object categories. The pattern of responses in SMG was  
462 not solely driven by the tool category as removing tools from the inanimate objects did not  
463 qualitatively change the results (data not shown).



464  
465  
466  
467  
468  
469  
470  
471  
472  
**Figure 2.** Univariate fMRI responses to dynamic and static stimuli averaged within animate and inanimate categories for each region of interest. Results do not qualitatively differ when removing the human and tool categories from the analysis.

473 Error bars represent standard errors.  
474



475 **Figure 3.** Univariate fMRI response preference for animate compared to inanimate object categories in  
476 dynamic and static stimuli for each region of interest. \* $p < 0.05$ . Error bars represent standard errors.  
477  
478

479 To better visualize and investigate the interaction between stimulus format and animacy,  
480 we subtracted inanimate responses from animate responses to produce a measure of animacy  
481 preference within each stimulus format (Figure 3). Unpaired t-tests evaluating animacy  
482 preference against 0 revealed that there was no animacy preference in V1, inferior IPS, and the  
483 right SMG area in either stimulus format (dynamic:  $t_s < 1.56$ ,  $p_s > 0.21$ , Cohen's  $d_s < 0.42$ ,  
484 static:  $t_s < 0.76$ ,  $p_s > 0.55$ , Cohen's  $d_s < 0.20$ ). In contrast, for both stimulus formats, LO, pFS,  
485 and EBA showed a preference for animate categories (dynamic:  $t_s > 3.15$ ,  $p_s < 0.02$ , Cohen's  $d_s$   
486  $> 0.84$ , static:  $t_s > 5.05$ ,  $p_s < 0.0002$ , Cohen's  $d_s > 1.35$ ) while left SMG preferred inanimate  
487 categories (dynamic:  $t(14) = 5.59$ ,  $p = 0.0005$ , Cohen's  $d = 1.49$ ). LOT-biomotion had significant  
488 preference for animate categories in the static ( $t(14) = 3.97$ ,  $p = 0.003$ , Cohen's  $d = 1.06$ ) but not  
489 in the dynamic condition ( $t(14) = 1.14$ ,  $p = 0.31$ , Cohen's  $d = 0.31$ ). All regions showed a  
490 preference in the same direction for dynamic and static conditions.

491 pFS and left SMG further showed a significant difference in the magnitude of their  
492 animacy preference across formats. pFS, a ventral region known to be involved in object  
493 recognition, showed a stronger preference for animate object stimuli in the static compared to the  
494 dynamic condition (paired t-test:  $t(14) = 3.07$ ,  $p = 0.03$ , Cohen's  $d = 0.79$ ), while left SMG, a  
495 parietal region thought to be involved in tool processing and action observation had a stronger  
496 preference for inanimate object stimuli in the dynamic compared to the static condition (paired t-  
497 test:  $t(14) = 3.73$ ,  $p = 0.02$ , Cohen's  $d = 0.96$ ). These significant interactions between stimulus  
498 format and animacy preference suggest that the category preference responses in pFS and left  
499 SMG are modulated by the format through which the category information is provided. The most  
500 ventral region, pFS, is more sensitive to static form presentations of animate objects and the most  
501 dorsal lateral region, left SMG, is more sensitive to dynamic motion information about inanimate  
502 objects.

503

#### 504 **Effect of stimulus format on multivariate object category representations**

505 We next examined the multivariate patterns of each of our regions of interest to further  
506 explore how object category information is represented in the brain when sourced from dynamic  
507 movements and static images. We first sought to test if each of our regions contained information  
508 about the 6 object categories within each stimulus format. To do this, we calculated average  
509 pairwise classification accuracy for the 6 object categories for the static and dynamic conditions  
510 using a linear SVM classifier (Chang and Lin, 2011). Figure 4a shows the pooled results of this  
511 analysis across subjects. Unpaired t-tests revealed that the object categories were decoded  
512 significantly above chance in both dynamic and static formats in all regions but V1 (dynamic:  $t_s$   
513  $> 7.04$ ,  $ps < 0.00001$ , Cohen's  $ds > 1.82$ ; static:  $t_s > 2.73$ ,  $ps < 0.02$ , Cohen's  $ds > 0.71$ ). In V1,

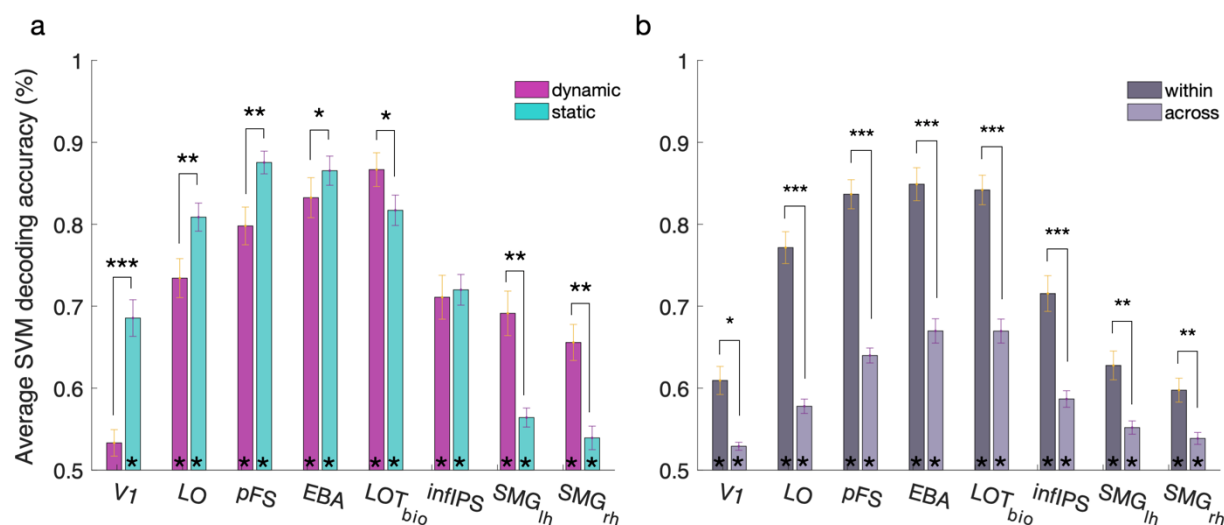
514 significant decoding was only found in the static stimulus condition (static:  $t(14) = 8.31$ ,  $p =$   
515  $0.00001$ , Cohen's  $d = 2.15$ ; dynamic:  $t(14) = 2.05$ ,  $p = 0.06$ , Cohen's  $d = 0.53$ ). In all regions but  
516 infIPS, there were significant differences between the decoding accuracies across stimulus  
517 format (infIPS:  $t(14) = 0.59$ ,  $p = 0.57$ , Cohen's  $d = 0.15$ ). In V1, LO, pFS, and EBA decoding  
518 accuracies were higher in the static condition than the dynamic ( $ts > 2.32$ ,  $ps < 0.001$ , Cohen's  $ds$   
519  $> 0.60$ ), while in LOT-biomotion and bilateral SMG, decoding accuracies were higher in the  
520 dynamic condition ( $ts > 3.24$ ,  $ps < 0.008$ , Cohen's  $ds > 0.84$ ).

521 To ensure that the significant decoding of object category from dynamic information was  
522 due to differences in the responses to object categories and not contingent upon optic flow  
523 information differences that were confounded with category in our stimulus set, we performed a  
524 control analysis in which we correlated the dynamic stimulus information with the multivariate  
525 fMRI responses (see Methods). No significant positive correlations were observed for any of the  
526 regions of interest ( $ts < 2.8$ ,  $ps > 0.06$ ).

527 We next used a cross-classification method to determine if abstract responses to object  
528 categories irrespective of stimulus format exist in our ROIs. The SVM classifier was trained in  
529 one stimulus format and then tested in the other format. Decoding accuracies when training on  
530 static and testing on dynamic and training on dynamic and testing on static were averaged to  
531 produce the light grey bars shown in Figure 4b. We also calculated the within-classification  
532 accuracy for training and testing within stimulus format (dark grey bars in Figure 4b; average of  
533 the two bars in Figure 4a). Significant cross-classification was observed in all regions of interest  
534 ( $ts > 5.31$ ,  $ps < 0.0001$ , Cohen's  $ds > 1.37$ ), and was significantly lower than within-  
535 classification in all ROIs ( $ts > 5.24$ ,  $ps < 0.0001$ , Cohen's  $ds > 1.35$ ). This suggests that the  
536 information about object categories in the multivariate pattern responses to the dynamic and



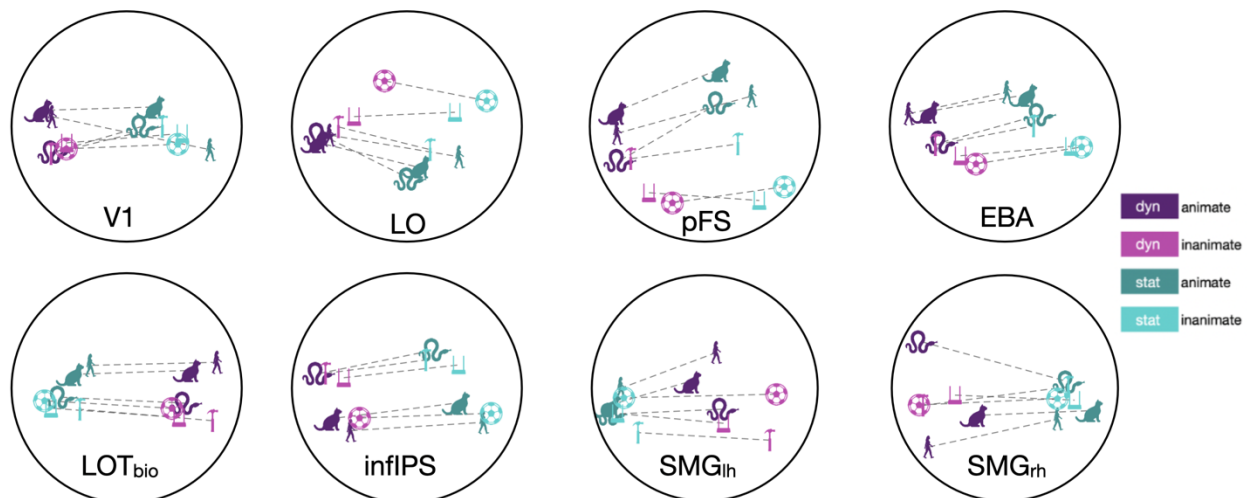
537 static stimuli was sufficiently similar to allow for significant decoding in one stimulus format  
 538 after being trained on the other.  
 539



540 **Figure 4.** Object category SVM decoding accuracies in each ROI. a) Average SVM decoding accuracies  
 541 when training and testing within the dynamic (pink) and static (teal) conditions. Asterisks within the bars  
 542 represent significance in t-tests against chance. All average decoding accuracies were significantly above  
 543 chance except for the dynamic condition in V1. Asterisks above bars represent paired t-tests across  
 544 format. In all regions but infIPS, accuracies were significantly higher for one of the formats—LO, pFS,  
 545 and EBA had significantly higher accuracy in the static condition while LOT-biomotion and bilateral  
 546 SMG had significantly higher accuracy in the dynamic condition. b) The within stimulus format decoding  
 547 accuracies, depicted in dark grey bars, were produced by averaging the dynamic and static decoding  
 548 accuracies in A. The cross-format decoding accuracies are shown in light grey bars. Cross classification  
 549 was significantly above chance in all regions of interest. Within classification was significantly higher  
 550 than cross classification in all regions of interest. Error bars represent standard errors. Asterisk notation: \*  
 551  $p < 0.05$ , \*\*  $p < 0.001$ , \*\*\*  $p < 0.0001$ .  
 552

553 To further visualize the similarity between the fMRI responses to the object categories in  
 554 the dynamic and static conditions, we calculated the pairwise Euclidean distances between the  
 555 patterns of responses to the 6 object categories and the two stimulus formats in each ROI. We  
 556 then performed a multidimensional scaling analysis on the resultant dissimilarity matrix and  
 557 visualized the first two dimensions in each of the regions of interest (Figure 5). In all regions,  
 558 there was a clear separation between the responses to the dynamic (shown in purple and pink)  
 559 and static stimuli (shown in green and teal). In addition, the ventro-temporal regions and inferior

560 parietal cortex showed a separation amongst the individual object categories. The nearly parallel  
561 lines connecting the dynamic and static conditions of the same category indicate that categories  
562 with responses that were similar to each other in one condition were also similar to each other in  
563 the other condition and is in line with the results of the cross-classification analysis performed  
564 earlier. In bilateral supramarginal areas, this object category separation was evident for the



565 dynamic stimulus responses, but the static stimulus responses remained clustered together. In  
566 V1, while there was a separation between dynamic and static, the arrangement of categories does  
567 not appear to be consistent across conditions.

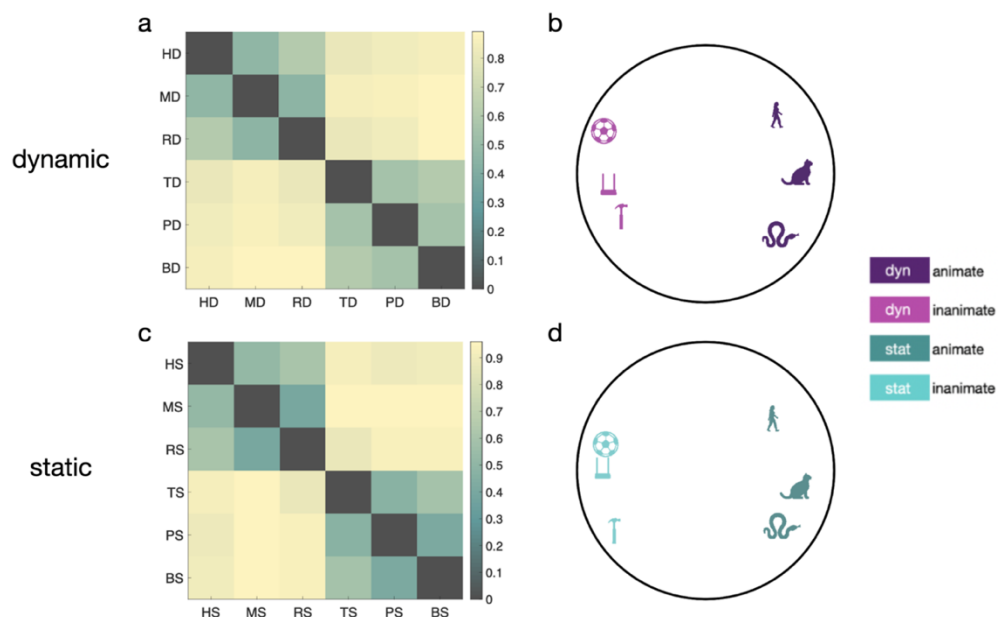
568 **Figure 5.** Multidimensional scaling visualization of fMRI response similarity between the object  
569 categories presented in the dynamic and static formats. MDS was performed on the similarity matrix  
570 obtained from the Euclidean distances of response patterns for the 12 conditions in each ROI. Dotted lines  
571 connect dynamic and static presentations of the same object category. The dynamic condition is signified  
572 by purple and the static condition is signified by green. Within each condition, the darker hues represent  
573 the animate categories while the lighter hues represent the inanimate categories. The 6 object categories  
574 are symbolized as with the following icons: human (person from side profile), mammal (cat), reptile  
575 (snake), tool (hammer)

### 576 577 **Odd-one-out behavioral experiment**

578 To investigate how the responses of each ROI to the 6 object categories in each format  
579 relates to the behavioral measure of similarity we performed two behavioral experiments on  
580 Amazon Mechanical Turk in which we showed participants three objects (either in static

581 condition or in dynamic condition) and asked them to judge the similarity between the three  
582 objects and pick the odd-one-out. We calculated two dissimilarity matrices based on the  
583 responses, one for the static stimuli and one for the dynamic stimuli (see Methods). We then  
584 averaged the individual object distances from each category to obtain dissimilarity scores  
585 between the 6 object categories for the two stimulus formats (Figure 6a). The reliability of these  
586 similarity judgments was evaluated for each stimulus format separately (see Methods).  
587 Participants rated both stimulus formats with highly stable similarity judgments ( $r = 0.98$  for  
588 both dynamic and static stimuli). We used multidimensional scaling on the pairwise  
589 dissimilarities of each stimulus format to visualize the distance between object categories in the  
590 first two dimensions (Figure 6b).

591 The dynamic and static similarity judgments had highly similar structure, showing a clear  
592 separation between animate and inanimate categories in the first dimension. The animate  
593 (human, mammal, and reptile) and inanimate (tool, pendulum/swing, and ball) categories were  
594 also separated from each other along the second dimension in both tasks. Overall, the  
595 dissimilarities from the dynamic and static tasks were highly correlated ( $r = 0.98$ ,  $p = 2.80e-10$ ),  
596 however, there also appeared to be slight qualitative differences in the arrangement of the



597 inanimate object categories along the second dimension.

598 **Figure 6.** Odd-one-out similarity judgements of dynamic and static stimuli at the category level. The  
599 matrices depict pairwise dissimilarity scores between object categories in dynamic (a) and static (c)  
600 stimulus formats. The circle plots represent the object categories project into the first two dimensions  
601 from multidimensional scaling on their dissimilarities in the dynamic (b) and static (d) stimuli.

602 To further explore the similarity structure of the dynamic and static stimuli at the  
603 exemplar level, a hierarchical clustering algorithm was used on the odd-one-out similarity  
604 judgments (Figure 7). Similar to the MDS of odd-one-out judgements at the category level, a  
605 gross distinction between animate and inanimate objects was observed for both the static and

606 dynamic conditions. Moreover, as in the MDS, the three object categories within  
607 the animate and inanimate superordinate categories are largely distinguished in both  
608 formats. However, the clustering algorithm also revealed several interesting differences in  
609 the similarity judgments of the same objects when presented in either static image or  
610 dynamic optic flow format. For example, the dynamic baboon stimulus, a clip of a baboon  
611 sitting and feeding, was grouped with the human stimuli, while the static baboon  
612 stimulus was grouped with the mammal stimuli. Similarly, the dynamic presentation of  
613 the two pendulum stimuli were grouped with the swings, presumably due to their shared  
614 movement patterns, while their static presentations were grouped with the balls,  
615 likely due to their shared global form. These deviations of specific exemplars from their

616 category clusters illustrate important differences in the category information provided by  
617 dynamic and static visual cues and shed light on some of the heuristics that are used to guide  
618 similarity judgments in the absence of either form or motion information. When luminance-  
619 defined edges are not available, robust category information can be derived from dynamic  
620 motion-isolated inputs.

621  
622

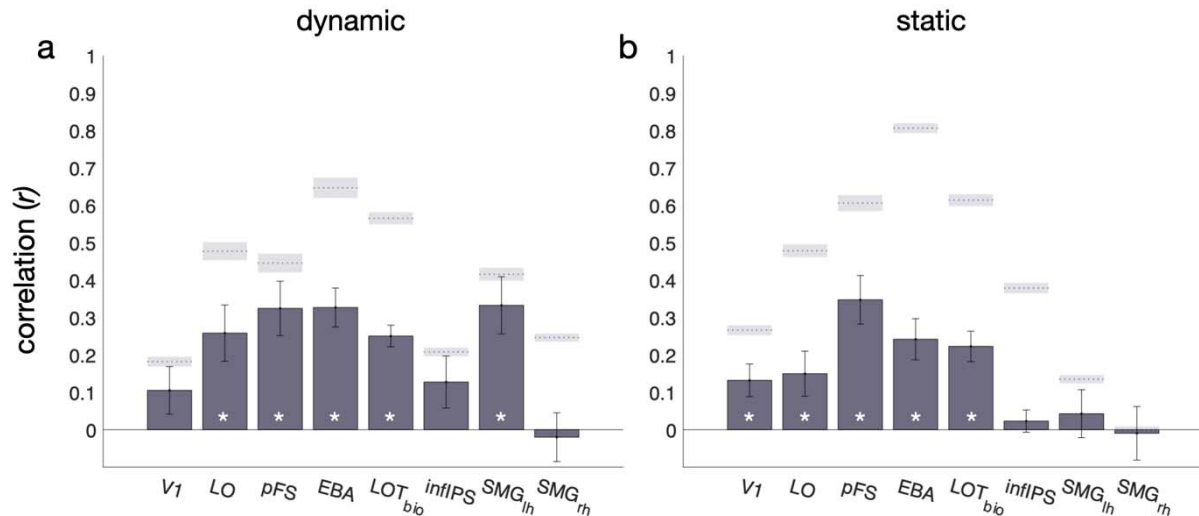
623 **Figure 7.** Hierarchical clustering of odd-one-out similarity judgments of the dynamic and static stimuli at  
624 the exemplar level. Edited versions of the static stimuli were used to visualize the similarity structure of  
625 both the dynamic (top) and static (bottom) stimuli as category of the dynamic stimuli cannot be gleaned  
626 from individual frames. The scale and position of the objects are not representative of the stimuli during  
627 presentation. Stimulus borders were colored to distinguish the six object categories. The human stimulus  
628 examples were modified into two-tone images for this figure to deidentify the individuals in the stimuli.  
629

630 To investigate how the object category fMRI responses to each format relate to  
631 behavioral judgements of similarity, we correlated the dissimilarity scores from the dynamic and  
632 static behavioral experiments (dynamic and static reliability: 0.985) to those obtained from the  
633 Euclidean distances between the multivariate response patterns in each region of interest (*rs*:  
634 dynamic > 0.03; static > 0.02, apart from right SMG, see below). As shown in Figure 8, most  
635 ventral and lateral temporal regions—LO, pFS, EBA, LOT-biomotion—showed significant  
636 correlations with the object similarity judgments for both the dynamic and static stimuli  
637 (dynamic:  $p < 0.01$ ; static:  $p < 0.05$ ). The responses in infIPS were not correlated to object  
638 similarity judgments for either the dynamic or static stimuli (dynamic:  $p = 0.12$ , static:  $p = 0.59$ ).  
639 The activity in left SMG was significantly correlated with the similarity judgments for the  
640 dynamic stimuli ( $p = 0.001$ ), but not for the static stimuli ( $p = 0.59$ ). Similarly, the activity in V1  
641 was significantly correlated with similarity judgments for the static stimuli ( $p = 0.02$ ), but not for  
642 the dynamic stimuli ( $p = 0.14$ ). The only significant difference between the correlations of the  
643 behavioral similarity judgments and the fMRI responses to the two conditions was found in the  
644 left SMG area, in which the correlation was significantly higher with similarity judgments of the  
645 dynamic stimuli compared to the static stimuli ( $t(14) = 3.32$ ,  $p = 0.04$ , Cohen's  $d = 0.86$ ). In the  
646 right SMG area, the  $r$  value was -0.0083 for the static condition, signifying a reliability of zero.  
647 As this suggests that the responses to the static stimuli in this region were unreliable, the  
648 correlation between the multivariate fMRI responses in the right SMG to the static stimuli with  
649 behavioral assessments of their similarity will not be interpreted.

650

651

652



653 **Figure 8.** Correlation of Euclidean distance between multivariate fMRI responses and behavioral  
654 dissimilarity matrices for a) dynamic and b) static stimuli. \*  $ps < 0.05$ . Error bars represent standard  
655 errors. Shaded regions represent the average noise ceiling (dotted line) and the standard error of noise  
656 (shaded region) for each ROI.

657

## 658 Discussion

659 Motion is an important visual cue that can provide category-relevant information in the  
660 absence of luminance-defined edges and form. Here, we introduce a novel approach to  
661 systematically separate form and motion signals and study the contribution of the motion signal  
662 to object category processing in isolation. To our knowledge, our study is the first to use this  
663 approach to compare the neural processing of form and motion signals from several animate and  
664 inanimate object categories. We sought to determine whether category-relevant information from  
665 the two sources is shared across the visual system by comparing dynamic and static category  
666 processing in regions of interest across visual occipito-temporal and parietal cortices. The two  
667 highly dissimilar information sources produced distinct but overlapping representations of

668 animate and inanimate object categories, with a shift in processing primarily static information in  
669 more ventral regions to primarily dynamic information in more dorsal regions of cortex.

670

### 671 **Categorizing Objects with Motion Information**

672 An object identification task was used to determine whether our method for simulating  
673 the extracted motion information in dynamic flow fields could produce stimuli in which objects  
674 were recognizable. Our findings illustrate that, not only do people categorize motion-defined  
675 *animate* objects with high accuracy (Pinto, 2006; Pinto, 1994; Pavlova et al., 2001), this high  
676 performance also holds for three *inanimate* object categories: tools, swinging objects, and balls.  
677 These results extend previous research by showing that a wide range of objects spanning animate  
678 and inanimate categories can be recognized from just motion information. Our odd-one-out  
679 judgment task further demonstrated that the similarity judgments for the dynamic and static  
680 stimuli were highly correlated. This consistency suggests that people infer the similarity of  
681 objects from the two sources of information in a similar way.

682 When discussing the perception of objects from motion, it is important to distinguish  
683 between two types of information that can be gleaned from motion cues: 1) structure from  
684 motion, a percept of a form arising from the global integration of coherent local motion vectors,  
685 and 2) types of actions that are diagnostic of a particular object category such as walking,  
686 swinging, tool use, bouncing, etc. Though it was not within the scope of this study to  
687 systematically distinguish these two sources, the exemplar level clustering of our odd-one-out  
688 data qualitatively suggests that both factors may play an important role in subjects' judgements  
689 of object similarity. For example, images of pendulums and bouncing balls maybe judged to be

690 similar since they both contain a round shape, but distinct in dynamic form because they move  
691 differently.

692

693

694

### 695 **Format-dependent processing of object categories**

696 Comparison of the object category information across the two stimulus formats revealed  
697 differences in many of our regions of interest. Our findings suggest that stimulus format matters  
698 for: 1) processing of animate and inanimate objects—indicated by the regions of interest with  
699 significant interactions between stimulus format and univariate animacy preference (i.e., pFS and  
700 left SMG)—and 2) discriminating object categories within format—indicated by regions with  
701 significant differences in the multivariate classification accuracy of the responses to dynamic and  
702 static stimuli (i.e., all regions but infIPS). Broadly speaking, we found that the most ventral and  
703 posterior regions we examined (LO, EBA, and pFS) showed higher classification in the static  
704 condition, while most dorsal and anterior regions (LOT-biomotion and bilateral SMG) had  
705 stronger classification in the dynamic condition. Interestingly, infIPS used both sources of  
706 information without dominance of one source over the other. Importantly, all regions of interest  
707 but V1 showed robust responses to, and significant decoding accuracies of, all categories  
708 presented in both static image and dynamic motion formats. Thus, differential multivariate  
709 processing of object category based on stimulus format in these regions is a matter of degree.  
710 These results align with predictions from the model presented by Giese and Poggio (2003), in  
711 which form and motion signals are processed by distinct neural populations that largely overlap  
712 in topographic regions across ventral and dorsal cortex.



713

## 714 **Animate and Inanimate Category Processing**

715           Relative to static images, investigation of topographic organization of object category  
716 processing driven by motion information has been largely neglected. However, an important  
717 exception can be found in the work of Beauchamp and colleagues (2003), in which they  
718 compared univariate fMRI responses between 1) full form videos and static images of humans  
719 and tools and 2) full form videos and point-light displays of humans and tools. Beauchamp et al.  
720 (2003) argued for two processing pathways—form and motion. Lateral temporal regions (STS  
721 and MTG), respond to their preferred category, humans and tools, respectively, in both PLDs and  
722 videos, suggesting category preference from motion without requiring form. Meanwhile, ventral  
723 temporal cortex (lateral and medial fusiform), needed form information for category preference  
724 responses. Our results are in agreement with these findings and demonstrate that the topography  
725 of animacy preference is not dependent on or exclusive to the human and tool categories—it also  
726 expands to other animate objects such as mammals and reptiles, and other inanimate objects such  
727 as pendulums/swings, and balls. These results suggest that large-scale animacy preference maps  
728 (Konkle & Caramazza, 2013, Sha et al., 2015) found with static objects in the brain might also  
729 be present for motion defined stimuli. Future studies with a larger stimulus set and sufficient  
730 power to perform whole-brain analyses will be crucial for expanding our findings beyond  
731 functionally defined regions of interest in VOTC and parietal cortex.

732

## 733 **Distinct but Overlapping Representations of Object Category for Dynamic and Static**

### 734 **Stimuli**

735           Using linear SVM classifiers, we decoded object category with high accuracy in all  
736 regions tested. In all regions but V1 and the right supramarginal area, both information sources  
737 drove object representations that were sufficiently distinguishable from each other to allow for  
738 high classification performance. Extracting form and motion information from the same objects  
739 and presenting them separately also allowed us to investigate the extent to which the  
740 representations are overlapping across stimulus formats. We used a cross-classification approach  
741 to identify regions that have format independent responses. A similar analysis has been used  
742 previously to study fMRI responses to human actions in full form videos and images (Hafri et al.,  
743 2017). Our results are largely in qualitative agreement with those of Hafri and colleagues, with  
744 the exception that we found significantly more widespread cross-classification, possibly because  
745 our static stimuli were source matched to our dynamic stimuli. Cross-decoding in all regions  
746 (apart from V1) suggests that the object category representations driven by static and dynamic  
747 information were sufficiently distinct to allow for significant within format classification, but  
748 also sufficiently overlapping that their shared information could lead to significant cross-  
749 classification. These results suggest the existence of abstract object category responses that pool  
750 information about object category across various cues in the visual input.

751

## 752 **Relationship between brain and behavior**

753           Multivariate responses to both the dynamic and static conditions in LO, pFS, EBA, and  
754 LOT-biomotion—the ventral and lateral regions—were correlated with the object similarity  
755 judgments of the dynamic and static stimuli, respectively, with no differences across condition.  
756 This implies that the fMRI responses in these regions follow the structure of the stimulus  
757 similarity characterized by our odd-one-out experiment. The only region to show a difference in

758 correlation across the stimulus conditions was the left supramarginal area, which showed higher  
759 correlations for the fMRI responses to the dynamic relative to the static stimuli. By contrast, the  
760 right supramarginal area showed no significant correlation to behavioral judgments of either  
761 condition, which indicates a lateralization of inanimate category processing to the left  
762 supramarginal area. This left lateralization has been shown previously in research on tool  
763 processing (Beauchamp et al., 2003). Importantly, not all regions that showed significant  
764 animacy preference or object category decoding had responses that were significantly correlated  
765 with the similarity structure of the behavioral judgments. In V1 and infIPS, the fMRI responses  
766 to both conditions were unrelated to the similarity judgments of both stimulus types, suggesting  
767 that these regions were extracting features irrelevant to similarity judgments on the objects.

768

## 769 **Conclusion**

770 In sum, our study demonstrates that in regions across occipito-temporal and parietal  
771 cortices, category responses driven by isolated motion signals parallel category responses to  
772 static form signals in a number of interesting ways. Regions that are traditionally considered part  
773 of the visual object recognition pathway that processes static information, such as the pFS, LO,  
774 and EBA, also extract robust object category information from isolated motion signals relevant  
775 to behavioral judgments of object similarity. Furthermore, cross-classification of object  
776 categories in all regions suggests that object-category information from static and dynamic  
777 signals overlap. Lastly, preferential processing of certain kinds of objects, such as animate or  
778 inanimate objects, is sensitive in some regions, i.e., the pFS and left SMG, to the format of visual  
779 information. Using the stimulus generation approach we have introduced, future studies can  
780 expand beyond the six object categories tested here and introduce parametric manipulations of

781 dimensions that are likely to play an important role in differential processing of motion-derived  
782 object categories. Candidate dimensions include the type of action or movements that the objects  
783 are performing as well as the orientation from which the movements are viewed. Such studies  
784 will be important for furthering our understanding of how various visual cues to object-category  
785 are processed and integrated together to form rich and robust object representations in the human  
786 brain.

## 787 **References**

- 788 1. Barclay, C. D., Cutting, J. E., & Kozlowski, L. T. (1978). Temporal and spatial factors in gait  
789 perception that influence gender recognition. *Perception & psychophysics*, 23(2), 145-152.
- 790 2. Bassili, J. N. (1978). Facial motion in the perception of faces and of emotional expression.  
791 *Journal of experimental psychology: human perception and performance*, 4(3), 373.
- 792 3. Beauchamp, M. S., Lee, K. E., Haxby, J. V., & Martin, A. (2003). FMRI responses to video and  
793 point-light displays of moving humans and manipulable objects. *Journal of cognitive*  
794 *neuroscience*, 15(7), 991-1001.
- 795 4. Benjamini, Y., & Hochberg, Y. (1995). Controlling the false discovery rate: a practical and  
796 powerful approach to multiple testing. *Journal of the Royal statistical society: series B*  
797 *(Methodological)*, 57(1), 289-300.
- 798 5. Bonda, E., Petrides, M., Ostry, D., & Evans, A. (1996). Specific involvement of human parietal  
799 systems and the amygdala in the perception of biological motion. *Journal of Neuroscience*,  
800 16(11), 3737-3744.
- 801 6. Brainard, D. H. (1997) The psychophysics toolbox. *Spatial Vision*. 10:433–436.
- 802 7. Chang, C. C., & Lin, C. J. (2011). LIBSVM: a library for support vector machines. *ACM*  
803 *transactions on intelligent systems and technology (TIST)*, 2(3), 1-27.
- 804 8. Cox, R. W. (1996). AFNI: software for analysis and visualization of functional magnetic  
805 resonance neuroimages. *Computers and Biomedical Research*, 29(3):162-173.  
806 doi:10.1006/cbmr.1996.0014
- 807 9. Cutting, J. E., Kozlowski, L. (1977) "Recognition of friends by their walk." *Bulletin of the*  
808 *Psychonomic Society*, 9, 353–356.
- 809 10. Desikan, R. S., Ségonne, F., Fischl, B., Quinn, B. T., Dickerson, B. C., Blacker, D., Buckner,  
810 R.L., ... & Killiany, R. J. (2006). An automated labeling system for subdividing the human  
811 cerebral cortex on MRI scans into gyral based regions of interest. *Neuroimage*, 31(3), 968-980.

- 812 11. Dittrich, W. H., Troscianko, T., Lea, S. E., & Morgan, D. (1996). Perception of emotion from  
813 dynamic point-light displays represented in dance. *Perception*, 25(6), 727-738.
- 814 12. Farnebäck, G. (2003, June). Two-frame motion estimation based on polynomial expansion. In  
815 Scandinavian conference on Image analysis (pp. 363-370). Springer, Berlin, Heidelberg.
- 816 13. Furl, N., Hadj-Bouziane, F., Liu, N., Averbeck, B. B., & Ungerleider, L. G. (2012). Dynamic and  
817 static facial expressions decoded from motion-sensitive areas in the macaque monkey. *Journal of*  
818 *Neuroscience*, 32(45), 15952-15962.
- 819 14. Giese, M. A., & Poggio, T. (2003). Neural mechanisms for the recognition of biological  
820 movements. *Nature Reviews Neuroscience*, 4(3), 179-192.
- 821 15. Giese, M. A. (2013). Biological and body motion perception. The Oxford handbook of perceptual  
822 organization, 575-596.
- 823 16. Grossman, E. D., & Blake, R. (2002). Brain areas active during visual perception of biological  
824 motion. *Neuron*, 35(6), 1167-1175.
- 825 17. Hafri, A., Trueswell, J., & Epstein, R. (2017) Neural Representations of Observed Actions  
826 Generalize across Static and Dynamic Visual Input. *Journal of Neuroscience* 37(11): 3056-3071.
- 827 18. Hirai, M., & Hiraki, K. (2006). The relative importance of spatial versus temporal structure in the  
828 perception of biological motion: an event-related potential study. *Cognition*, 99(1), B15-B29.
- 829 19. Ishai, A., Ungerleider, L. G., Martin, A., Schouten, J. L., & Haxby, J. V. (1999). Distributed  
830 representation of objects in the human ventral visual pathway. *Proceedings of the National*  
831 *Academy of Sciences*, 96(16), 9379-9384.
- 832 20. Johansson, G. (1976). Spatio-temporal differentiation and integration in visual motion perception.  
833 *Psychological research*, 38(4), 379-393.
- 834 21. Johansson, G. (1973) "Visual perception of biological motion and a model of its analysis"  
835 *Perception & Psychophysics*, 14, 201-211.
- 836 22. Kaiser, M. D., Shiffrar, M., & Pelphrey, K. A. (2012). Socially tuned: Brain responses  
837 differentiating human and animal motion. *Social neuroscience*, 7(3), 301-310.

- 838 23. Kleiner, M., Brainard, D., Pelli, D. (2007) “What’s new in Psychtoolbox-3?” *Perception*, 36,  
839 ECVF Abstract Supplement.
- 840 24. Konkle, T., & Caramazza, A. (2013). Tripartite organization of the ventral stream by animacy and  
841 object size. *Journal of Neuroscience*, 33(25), 10235-10242.
- 842 25. Kundu, P., Inati, S.J., Evans, J.W., Luh, W.M. & Bandettini, P.A. (2012). Differentiating BOLD  
843 and non-BOLD signals in fMRI time series using multi-echo EPI. *NeuroImage*, 60, 1759-1770.
- 844 26. Mitchell TM, Hutchinson R, Niculescu RS, Pereira F, Wang XR, Just M, Newman S (2004)  
845 Learning to decode cognitive states from brain images. *Machine Learning* 57:145–175.
- 846 27. Mather, G., & West, S. (1993). Recognition of animal locomotion from dynamic point-light  
847 displays. *Perception*, 22(7), 759-766.
- 848 28. Papeo, L., Wurm, M. F., Oosterhof, N. N., & Caramazza, A. (2017). The neural representation of  
849 human versus nonhuman bipeds and quadrupeds. *Scientific reports*, 7(1), 1-8.
- 850 29. Pavlova, M., Krägeloh-Mann, I., Sokolov, A., & Birbaumer, N. (2001). Recognition of point-light  
851 biological motion displays by young children. *Perception*, 30(8), 925-933.
- 852 30. Pavlova, M., Lutzenberger, W., Sokolov, A., & Birbaumer, N. (2004). Dissociable cortical  
853 processing of recognizable and non-recognizable biological movement: analysing gamma MEG  
854 activity. *Cerebral Cortex*, 14(2), 181-188.
- 855 31. Peissig, J. J., & Tarr, M. J. (2007). Visual object recognition: Do we know more now than we did  
856 20 years ago? *Annual Review of Psychology*, 58, 75-96.
- 857 32. Pinto, J. (1994). Human infants’ sensitivity to biological motion in pointlight cats. *Infant*  
858 *Behavior and Development*, 17, 871.
- 859 33. Pinto, J. (2006). “Developing body representations: A review of infants’ responses to biological-  
860 motion displays”. In *Perception of the human body from the inside out*, Edited by: Knoblich, G.,  
861 Grosjean, M., Thornton, I. and Shiffrar, M. 305–322.
- 862 34. Pinto, J., & Shiffrar, M. (2009). The visual perception of human and animal motion in point-light  
863 displays. *Social Neuroscience*, 4(4), 332-346.

- 864 35. Pitcher, D., Dilks, D. D., Saxe, R. R., Triantafyllou, C., & Kanwisher, N. (2011). Differential  
865 selectivity for dynamic versus static information in face-selective cortical  
866 regions. *Neuroimage*, *56*(4), 2356-2363.
- 867 36. Posse, S., Wiese, S., Gembris, D., Mathiak, K., Kessler, C., Grosse-Ruyken, M. L., Elghahwagi,  
868 B., ... & Kiselev, V. G. (1999). Enhancement of BOLD contrast sensitivity by single-shot  
869 multi-echo functional MR imaging. *Magnetic Resonance in Medicine: An Official Journal of the*  
870 *International Society for Magnetic Resonance in Medicine*, *42*(1), 87-97.
- 871 37. Ptito, M., Faubert, J., Gjedde, A., & Kupers, R. (2003). Separate neural pathways for contour and  
872 biological-motion cues in motion-defined animal shapes. *Neuroimage*, *19*(2), 246-252.
- 873 38. Saygin, A. P., Wilson, S. M., Hagler, D. J., Bates, E., & Sereno, M. I. (2004). Point-light  
874 biological motion perception activates human premotor cortex. *Journal of Neuroscience*, *24*(27),  
875 6181-6188.
- 876 39. Schenk, T., & Zihl, J. (1997). Visual motion perception after brain damage: II. Deficits in form-  
877 from-motion perception. *Neuropsychologia*, *35*(9), 1299-1310.
- 878 40. Scholl, B. J., & Gao, T. (2013). Perceiving animacy and intentionality: Visual processing or  
879 higher-level judgment. *Social perception: Detection and interpretation of animacy, agency, and*  
880 *intention*, *4629*, 197-229.
- 881 41. Schultz, J., & Bühlhoff, H. H. (2013). Parametric animacy percept evoked by a single moving dot  
882 mimicking natural stimuli. *Journal of vision*, *13*(4), 15-15.
- 883 42. Sha, L., Haxby, J. V., Abdi, H., Guntupalli, J. S., Oosterhof, N. N., Halchenko, Y. O., &  
884 Connolly, A. C. (2015). The animacy continuum in the human ventral vision pathway. *Journal of*  
885 *cognitive neuroscience*, *27*(4), 665-678.
- 886 43. Shepard, R. N. (1980) Multidimensional scaling, tree-fitting, and clustering. *Science* *210*:390 –  
887 398.



- 888 44. Virtanen, P., Gommers, R., Oliphant, T. E., Haberland, M., Reddy, T., Cournapeau, D., ... & Van  
889 Mulbregt, P. (2020). SciPy 1.0: fundamental algorithms for scientific computing in Python.  
890 *Nature methods*, 17(3), 261-272.